

Terahertz bolometric detectors based on graphene field-effect transistors with the composite h-BN/black-P/h-BN gate layers using plasmonic resonances

M. Ryzhii¹, V. Ryzhii², M. S. Shur³, V. Mitin⁴, C. Tang^{2,5}, and T. Otsuji²

¹*Department of Computer Science and Engineering,
University of Aizu, Aizu-Wakamatsu 965-8580, Japan*

²*Research Institute of Electrical Communication, Tohoku University, Sendai 980-8577, Japan*

³*Department of Electrical, Computer, and Systems Engineering,
Rensselaer Polytechnic Institute, Troy, New York 12180, USA*

⁴*Department of Electrical Engineering, University at Buffalo, SUNY, Buffalo, New York 14260 USA*

⁵*Frontier Research Institute for Interdisciplinary Sciences, Tohoku University, Sendai 980-8578, Japan*

We propose and analyze the performance of terahertz (THz) room-temperature bolometric detectors based on the graphene channel field-effect transistors (GC-FET). These detectors comprise the gate barrier layer (BL) composed of the lateral hexagonal-Boron Nitride black-Phosphorus/hexagonal-Boron Nitride (h-BN/b-P/h-BN) structure. The main part of the GC is encapsulated in h-BN, whereas a short section of the GC is sandwiched between the b-P gate BL and the h-BN bottom layer. The b-P gate BL serves as the window for the electron thermionic current from the GC. The electron mobility in the GC section encapsulated in h-BN can be fairly large. This might enable a strong resonant plasmonic response of the GC-FET detectors despite relatively lower electron mobility in the GC section covered by the b-P window BL. The narrow b-P window diminishes the Peltier cooling and enhances the detector performance. The proposed device structure and its operation principle promote elevated values of the room-temperature GC-FET THz detector responsivity and other characteristics, especially at the plasmonic resonances.

I. INTRODUCTION

The favorable band alignment of the graphene channel (GC) and the black-Arsenic_xPhosphorus_{1-x} (b-AsP) layers [1–4] enables new opportunities for electron and optoelectronic device applications. In particular, we recently proposed the terahertz (THz) bolometric detectors based on the field-effect transistors (FETs) with the b-AsP gate barrier layer (BL) and the metal gate (MG) [5, 6]. The operation of such bolometric detectors is associated with the heating of the two-dimensional electron (hole) system (2DEG) by the THz radiation resulting in the reinforcement of the thermionic electron emission from the GC to the MG via the b-AsP BL. The resonant excitation of the plasmonic oscillations in the GC [7–9] can result in a substantial rise of the electron heating efficiency and can lead to improvement of the detector characteristics, in particular, enhancement of the detector responsivity. However, the plasmonic resonances are sensitive to electron scattering, limiting the sharpness of the resonances and the responsivity peaks. This problem is linked to the prospects of elevating the room temperature mobility of the GCs contacted with the b-AsP BLs.

In this paper, we propose and evaluate the room-temperature THz bolometric detectors based on the GC-FETs, in which the thermionic electron current passes through a relatively narrow b-P collector window in the primarily h-BN gate BL. The main part of the GC/BL interface is made of h-BN, so the GC exhibits higher electron mobility in comparison with the GC covered by the b-P gate BL [10–15]. Using the composite h-BN/b-AsP/h-BN gate BL, one can improve the GC-FET detector performance due to:

(i) a substantial decrease in the plasmonic oscillations

damping;

(ii) a weaker hot electron energy flux from the GL via the b-P collector window resulting in the diminishing of the Peltier cooling of the 2DEG [16] because of a smaller length of the b-P section of the BL.

As shown in the following, these features of the GC-FETs with the composite gate BL enable a marked enhancement of the detector performance.

II. GC-FET BOLOMETRIC DETECTOR DEVICE STRUCTURE

Figure 1 shows the structures of the GC-FET bolometric detectors with different BLs and MGs. The structure of the GC-FET with the uniform b-P gate BL [see Fig. 1(a)] was considered previously [8, 15]. Here, we focus on the GC-FET bolometric detectors operating at room temperature with the composite BLs, schematically shown in Fig. 1(b). The devices with the structures seen in Fig. 1(c) are briefly discussed in the Comments section. The structure of the GC-FET bolometric detectors under consideration [see Fig. 1(b)] comprises the n-doped GC sandwiched between the substrate (h-BN) and the h-BN gate BL with a narrow b-P window. This structure is covered by the MG and supplied by the side contacts (corresponding to the FET source and drain). The length of the collector window $2L_C$ is smaller than the length of the GC $2L$. Figure 2 shows these GC-FET bolometric detectors band diagram (in the direction z perpendicular to the layers). The relatively low energy barrier for the electrons in the GL enables thermionic emission (in the region $|x| < L_C$) above the energy barrier at the GC/b-P interface. In contrast, this energy barrier in the regions

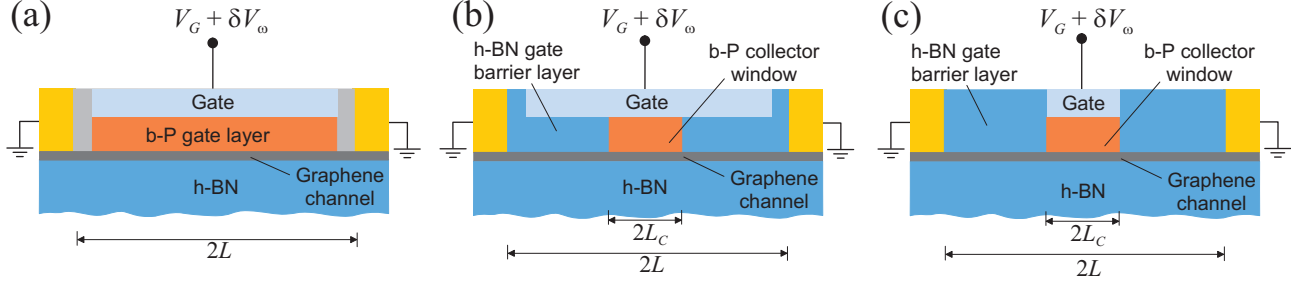


FIG. 1. Schematic views of the GC-FET bolometric detector structures with (a) the b-P gate BL [6, 15], (b) the composite h-BN/black-AsP/h-BN gate BL, and (c) the composite gate BL but with shortened MG.

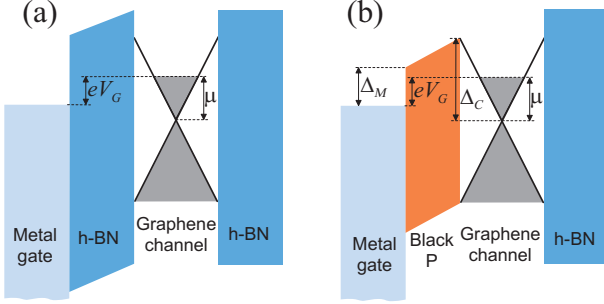


FIG. 2. The band diagrams of the GC-FET with the composite gate BL [shown in Fig. 1(b)] at its different cross-sections (a) $L_C < |x| < L$, i.e., in the region when the gate BL consists of the h-BN and (b) $|x| < L_C$ (in the collector window).

$L_C < |x| < L$ is fairly high, preventing electron emission from this section of the GC.

We assume that the sufficiently high GC doping level provides at the bias voltage $V_G = 0$ the flat-band condition $\Delta_M = \Delta_C - \mu_D$. Here Δ_M and Δ_C are the pertinent band offsets, $\mu_D = \hbar v_W \sqrt{\pi \Sigma_D}$ is the electron Fermi energy in the GC, where $v_W \simeq 10^8$ cm/s is the electron velocity in GCs, Σ_D is the donor density in the GC (or the density of the remote donors in the substrate near the GC), and \hbar is the Planck constant. In the GC-FETs under consideration with the Al MG, $\Delta_M = 85$ meV and $\Delta_C = 225$ meV, so that $\mu_D = 140$ meV, as shown in Table I. The latter occurs at $\Sigma_D \simeq 1.6 \times 10^{12}$ cm $^{-2}$ (see Ref. [8] and the references therein). When $V_G > 0$, the bottom of the b-P BL conduction band is somewhat inclined, as shown in Fig. 2(b). Below we consider the GC-FETs with not too thin BLs in the range of relatively low bias voltages, so that the electron tunneling through the BLs is negligible.

Apart from the bias voltage $V_G \geq 0$, the signal voltage $\delta V_\omega \exp(-i\omega t)$ generated by the THz radiation received by an antenna is applied between the GL and the MG. Here δV_ω and ω are the amplitude and frequency of the THz signal. This connection corresponds to the contact of one antenna lead with the MG and another with both the GC-FET side contacts. The signal voltage excites the ac current along the GC, resulting in electron heating in

the GC. The latter stimulates thermionic emission from the GC over the b-P section of the BL.

III. RECTIFIED CURRENT

The variation of the rectified thermionic gate current, $\langle \delta J_\omega \rangle$, associated with the incoming THz signal (and averaged over its period and serving as the detector output signal) is presented in the following form:

$$\langle \delta J_\omega \rangle = j^{\max} F H \int_{-L_C}^{L_C} dx \frac{\langle \delta T_\omega \rangle}{T_0}. \quad (1)$$

Here $F = \left(\frac{\Delta_C - \mu}{T_0} \right) \exp\left(-\frac{\Delta_C - \mu}{T_0} \right)$, j^{\max} is the maximal value of the current density from the GC to the MG via the b-P BL, T_0 is the lattice temperature, $\langle \delta T_\omega \rangle$ is the averaged electron effective temperature variation, and H is the GC width. The maximal electron current density j^{\max} is given by $j^{\max} = e \Sigma / \tau_\perp$, where $\Sigma \simeq \Sigma_D$ is the electron density in the GC, τ_\perp is the electron try-to-escape time, $\mu \simeq \mu_D$ is the electron Fermi energy, and e is the electron charge.

IV. ELECTRON ENERGY BALANCE IN THE GC AND AC EFFECTIVE TEMPERATURE

The spatial distribution (along the axis x) of $\langle \delta T_\omega \rangle$, is described by the one-dimensional electron heat transport equation, which for the device structure under consideration is presented in the following form [15]:

$$-h \frac{d^2 \langle \delta T_\omega \rangle}{dx^2} + \frac{\langle \delta T_\omega \rangle}{\tau_\varepsilon} = \frac{\langle Q_\omega \rangle}{\Sigma}. \quad (2)$$

Here $h \simeq v_W^2 / 2\nu$ is the electron thermal conductivity in the GC per electron (this corresponds to the Wiedemann-Franz relation), τ_ε is the electron energy relaxation time in the GC, $\langle Q_\omega \rangle = \text{Re } \sigma_\omega \langle |\delta E_\omega|^2 \rangle$ is the Joule power (per GC area unit) associated with the signal electric field, δE_ω , along the GC caused by the signal voltage at the

side contacts and amplified by the plasmonic effect, $\text{Re } \sigma_\omega = \sigma_0 \nu^2 / (\nu^2 + \omega^2)$, $\sigma_0 = e^2 \mu / \pi \hbar^2 \nu$ are the Drude ac and dc conductivities, and ν is the electron scattering frequency in the GC. Due to the smallness of the collector window length, we disregard the energy flux of the electrons transferring from the GC into the MG via this window (i.e., the Peltier cooling) [9, 15, 16] in comparison with the electron energy relaxation on phonons in the whole GC [17–21] and the heat absorbed by the side contacts (due to a high electron heat conductivity in GCs [22, 23]).

The quantity $\langle |\delta E_\omega|^2 \rangle$ is the square of ac electric field modulus averaged over the oscillations. Setting the boundary condition of the ac potential $\delta\varphi$ as

$$\langle \delta\varphi_\omega \rangle|_{x=\pm L} = \delta V_\omega, \quad (3)$$

and accounting for the excitation of plasmonic oscillations in the gated two-dimensional electron systems (neglecting the role of the short GC b-P region) one can obtain (see Appendix A)

$$\langle |\delta E_\omega|^2 \rangle = \frac{1}{2} \left(\frac{\delta V_\omega}{L} \right)^2 \left| \frac{\gamma_\omega \sin(\gamma_\omega x/L)}{\cos \gamma_\omega} \right|^2. \quad (4)$$

Here $\gamma_\omega = \pi \sqrt{\omega(\omega + i\nu)} / 2\Omega_P$ and $\Omega_P = (\pi e / \hbar L) \sqrt{\mu W / \kappa}$ are the effective wavenumber and the plasmonic frequency (corresponding to the symmetric conditions at the contacts), respectively, κ is the dielectric constant of the BLs, W is the GL thicknesses. The second term in the left-hand side of Eq. (2) is associated with the electron energy relaxation due to the interaction with phonons (mainly with the GC and interface phonons [17–21]), whereas the term in the right-hand side describes the Joule heating by the ac electric field induced by the potential variations at the side contacts (i.e., by the THz radiation).

Solving Eq. (2) with the boundary conditions

$$\langle \delta T_\omega \rangle|_{x=\pm L} = 0, \quad (5)$$

we obtain the following spatial distribution:

$$\langle \delta T_\omega \rangle = \left(\frac{v_W^2 \tau_\varepsilon}{\mu \nu} \right) \left\{ \frac{1 - \frac{\cos(\pi \omega x / \Omega_P L)}{1 + (\pi \varepsilon \omega / \Omega_P)^2}}{\sin^2(\pi \omega / 2\Omega_P) + (4\Omega_P / \pi \nu)^2 \cos^2(\pi \omega / 2\Omega_P)} - \left[1 - \frac{\cos(\pi \omega / \Omega_P)}{1 + (\pi \varepsilon \omega / \Omega_P)^2} \right] \frac{\cosh(x/L\varepsilon)}{\cosh(1/\varepsilon)} \right\} \left(\frac{e\delta V_\omega}{L} \right)^2. \quad (6)$$

Figure 3 shows the spatial distributions of the temperature signal component $\langle \delta T_\omega \rangle$ obtained using Eq. (6) for different ratios, ω / Ω_P , of the signal frequency and the plasmonic frequency. It is seen that the deviation of the signal frequency from the plasmonic frequency leads to a marked weakening of the electron heating. The dependences of the $\langle \delta T_{\Omega_P} \rangle|_{x=0}$ (in the GC center) versus the GC length $2L$ for different values of the electron collision frequency ν are plotted in Fig. 4. The behavior of these plots is associated with the specifics of the ac electric field distribution (this field is a relatively small in the GC center leading to a decrease of the average field with increasing L , and the dependence of the electron heat conductivity h on ν). As follows from Eq. (6), $\langle \delta T_{\Omega_P} \rangle|_{x=0} \propto \bar{\Pi}_{\Omega_P} / \nu$, where

$$\bar{\Pi}_\omega = 1 - \frac{1}{1 + (\pi \varepsilon \omega / \Omega_P)^2} - \left[1 - \frac{\cos(\pi \omega / \Omega_P)}{1 + (\pi \varepsilon \omega / \Omega_P)^2} \right] \frac{1}{\cosh(1/\varepsilon)} \quad (7)$$

and the parameter $\varepsilon = \sqrt{\hbar \tau_\varepsilon} / L = v_W \sqrt{\tau_\varepsilon / 2\nu} / L$ characterize the electron system cooling at the side contacts. The factor $\bar{\Pi}_\omega$ and, hence, $\bar{\Pi}_{\Omega_P}$ exhibit a pronounced variation with varying ν and L (via the dependence of ε on ν and L), which leads to the features of Fig. 4.

V. DETECTOR RESPONSIVITY

Equations (1) and (6) result in

$$\frac{\langle \delta J_\omega \rangle}{2HL_C} = \frac{e\mu}{\pi \hbar^2 \nu T_0} \left(\frac{\tau_\varepsilon F}{\tau_\perp} \right) \left(\frac{e\delta V_\omega}{L} \right)^2 \times \frac{\bar{\Pi}_\omega}{[\sin^2(\pi \omega / 2\Omega_P) + (4\Omega_P / \pi \nu)^2 \cos^2(\pi \omega / 2\Omega_P)]}. \quad (8)$$

We use the following definition of the GC-FET bolometric detector voltage responsivity: $R_\omega^V = \langle \delta J_\omega \rangle \rho_L / S_\omega$, where ρ_L is the load resistance, and S_ω is the THz power collected by the detector antenna.

The dark current is given by [15]

$$J^{dark} = \frac{2HL_C}{\pi} \left(\frac{\mu}{\hbar v_W} \right)^2 \exp\left(-\frac{\Delta_M}{T_0}\right) \left(\frac{e}{\tau_\perp} \right) \times \exp\left(\frac{\mu_0}{(\mu_0 + \mu_D)} \frac{eV_G}{T_0}\right) \left[1 - \exp\left(-\frac{eV_G}{T_0}\right) \right] \simeq \frac{2HL_C}{\pi} \left(\frac{\mu_D}{\hbar v_W} \right)^2 \exp\left(-\frac{\Delta_M}{T_0}\right) \left(\frac{e^2 V_G}{\tau_\perp T_0} \right), \quad (9)$$

where $\mu_0 = \kappa \hbar^2 v_W^2 / 4e^2 W$. Here we accounted for that at $\mu \simeq \mu_D + \mu_0 eV_G / (\mu_0 + \mu_D)$. Considering Eq. (9), we

TABLE I. Parameters of the GC-FET detectors with h-BN/b-AP/h-BN gate BL and Al MG.

Δ_C (meV)	Δ_M (meV)	μ_D (meV)	L (μm)	L_C (μm)	W (nm)	$\Omega_P/2\pi$ (THz)	ν^{-1} (ps)	τ_ε (ps)	τ_\perp (ps)
225	85	140	1.0	0.05 - 0.15	32 - 72	1.0 - 1.5	0.25 - 1.0	10	10

find that at $eV_G \simeq T_0 \ll e\bar{V}_G$ (where $\bar{V}_G = T_0(\mu_0 + \mu_D)/e\mu_0$),

$$\rho_L = \rho \simeq \frac{\pi}{2HL_C} \exp\left(\frac{\Delta_M}{T_0}\right) \left(\frac{\hbar v_W}{\mu_D}\right)^2 \left(\frac{\tau_\perp T_0}{e^2}\right). \quad (10)$$

Accounting for that the antenna aperture $A_\omega = \lambda_\omega^2 g/4\pi$, where λ_ω is the THz radiation wavelength and g is the antenna gain [24], for the relation between $|\delta V_\omega|^2$ and the collected power we obtain $|\delta V_\omega|^2 = 32S_\omega/gc$, where c is the speed of light in vacuum. Using the latter and invoking Eq. (7), we obtain

$$R_\omega^V = \frac{R^V \bar{\Pi}_\omega}{\sin^2(\pi \omega/2\Omega_P) + (4\Omega_P/\pi\nu)^2 \cos^2(\pi \omega/2\Omega_P)}, \quad (11)$$

where

$$\begin{aligned} R_V &= \frac{32}{137g} \left(\frac{\hbar}{eT_0}\right) \left(\frac{\Delta_M}{\mu}\right) \left(\frac{v_W^2 \tau_\varepsilon}{L^2 \nu}\right) \\ &= \frac{32}{137g} \left(\frac{\hbar \Delta_M}{e^2 T_0}\right) \left(\frac{\tau_\varepsilon \mathcal{M}}{L^2}\right) \end{aligned} \quad (12)$$

is the responsivity characteristic value. Here \mathcal{M} is the electron mobility in the GC. At $\nu < \Omega_P$ the denominator in the right-hand side describes the resonant frequency dependence of R_ω^V [with maxima of the latter at $\omega \simeq \Omega_P(2n - 1)$, $n = 1, 2, 3, \dots$ is the resonance index]. The quantity $R_{\Omega_P}^V = R^V \bar{\Pi}_{\Omega_P}$ is equal to the maximal voltage responsivity at the fundamental resonance $\omega = \Omega_P$ [see Eq. (7)]. It is instructive that R^V is independent of the length of the collecting window $2L_C$ and the try-to-escape time τ_\perp .

Using the device structure parameters for the detector structure with $\nu = 2/\text{ps}$, $L_C = 0.1 \mu\text{m}$, $H = 2 \mu\text{m}$, and $g = 1.6$ (other parameters are listed in Table I), and accounting for Eqs. (9) - (11), for the resonant responsivity we obtain $R_{\Omega_P}^V \simeq 7 \times 10^3 \text{ V/W}$.

VI. DETECTOR NOISE EQUIVALENT POWER AND DARK CURRENT LIMITED DETECTIVITY

Using Eqs. (9) and (11), we arrive at the following expressions for the GC-FET noise equivalent power (NEP) and the dark-current-limited detectivity (D^*) at the fundamental plasmonic resonance ($n = 1$):

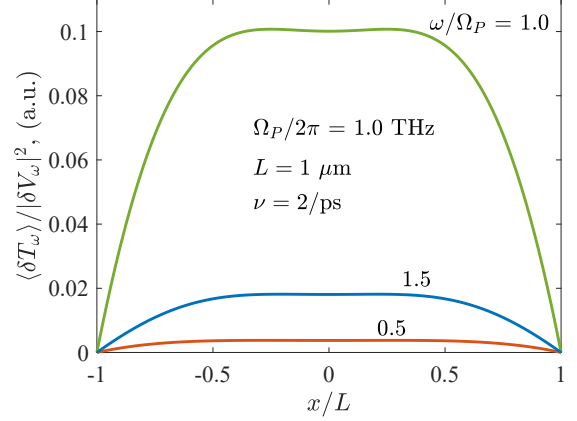


FIG. 3. Spatial distribution of the electron temperature variation caused by THz radiation with different frequencies.

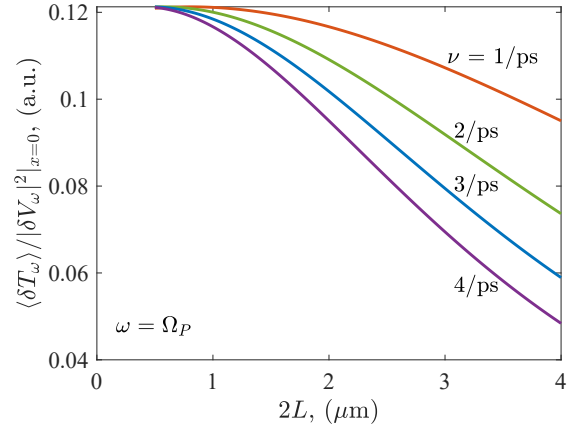


FIG. 4. Electron temperature variation at the GC center ($x = 0$) as a function of the GL length $2L$ calculated for different values of the electron collision frequency ν (different values of the electron heat conductivity h : 5, 5/2, 5/3, 5/4 $\times 10^3 \text{ cm}^2/\text{s}$) at $\omega = \Omega_P$.

$$\begin{aligned} \text{NEP} &\simeq \frac{137\sqrt{2}\pi g L^2}{64\sqrt{2}L_C H} \left(\frac{\sqrt{\tau_\perp} \nu T_0}{v_W \tau_\varepsilon}\right) \\ &\times \left(\frac{2T_0}{\Delta_M}\right) \exp\left(\frac{\Delta_M}{2T_0}\right) \frac{1}{\bar{\Pi}_{\Omega_P}}, \end{aligned} \quad (13)$$

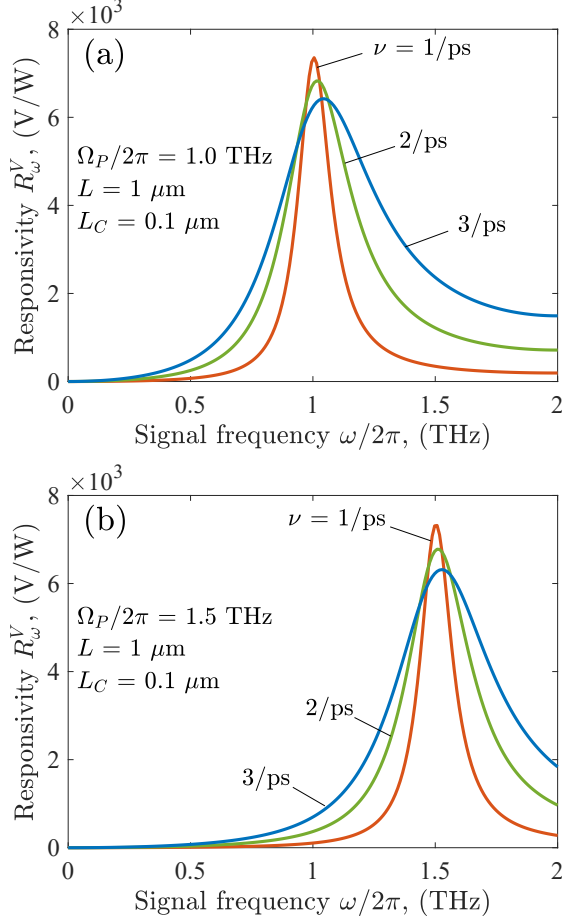


FIG. 5. Spectral characteristics of the voltage responsivity R_ω^V (in the frequency range around the fundamental resonance) for different values of collision frequency ν calculated for GC-FETs with different plasmonic frequencies (a) $\Omega_P/2\pi = 1$ THz and (b) $\Omega_P/2\pi = 1.5$ THz.

$$D^* = \frac{64(2L_C H)}{137\sqrt{2\pi} g L^2} \left(\frac{v_W \tau_\varepsilon}{\sqrt{\tau_\perp} \nu T_0} \right) \times \left(\frac{\Delta_M}{2T_0} \right) \exp\left(-\frac{\Delta_M}{2T_0}\right) \bar{\Pi}_{\Omega_P}, \quad (14)$$

respectively, where

$$\bar{\Pi}_{\Omega_P} = 1 - \frac{1}{1 + (\pi \varepsilon)^2} - \left[1 + \frac{1}{1 + (\pi \varepsilon)^2} \right] \frac{1}{\cosh(1/\varepsilon)}.$$

The estimates for NEP and D^* of the GC-FET detector with the same parameters as those used for the estimation of $R_{\Omega_P}^V$ yield $NEP \sim 1$ pW/ $\sqrt{\text{Hz}}$ and $D^* \sim 6 \times 10^7$ cm $\sqrt{\text{Hz}}$ /W. These values are about or exceeding the characteristics of other uncooled THz bolometers (see, for example, Refs. [25] and [26]).

Figure 7 shows NEP and D^* as functions of ν calculated for the GC-FETs with different lengths, L_C , of the collector window.

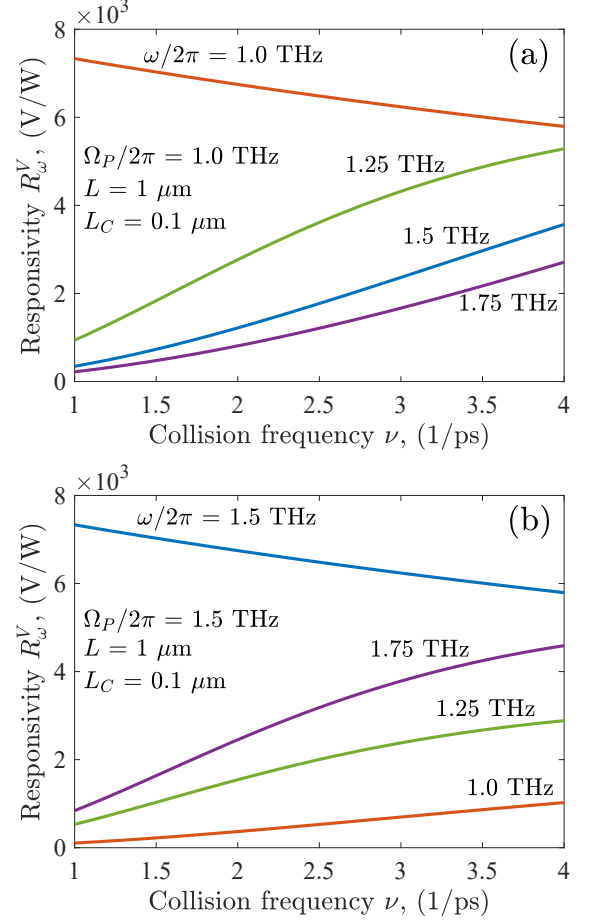


FIG. 6. Voltage responsivity R_ω^V versus collision frequency ν at different signal frequencies $\omega/2\pi$ calculated for the GC-FETs with (a) $\Omega_P/2\pi = 1$ THz and (b) $\Omega_P/2\pi = 1.5$ THz. The top lines correspond to the fundamental plasmonic resonances.

VII. COMMENTS

Calculating Eq. (9), we disregarded the variation of μ with increasing bias voltage V_G at not too large bias voltages, $\mu \simeq \mu_D + \mu_0 eV_G/(\mu_0 + \mu_D) \simeq \mu_D$. For $\kappa = 4$ and the same other parameters as above, $\mu_0 \simeq (6.8 - 13.6)$ meV and $\bar{V}_G \simeq (283 - 541)$ meV. Hence, at $eV_G \lesssim T_0$, one obtains $(R_\omega^V/R_\omega^V|_{V_G=0} - 1) \simeq (4.6 - 8.8)\%$.

According to Eq. (9), the dark current $J^{dark} = eV_G/\rho$, where ρ is given by Eq. (10). Taking this into account, in particular, for the ratio of D^* in a wide range of V_G and D^* at $eV_G = T_0$ given by Eq. (14) we obtain $D^*/D^*|_{eV_G=T_0} \simeq \sqrt{T_0/eV_G}$. It is worth noting that at smaller gate voltages $eV_G < T_0$, the detector detectivity might be limited not by the dark current, but by the Johnson-Nyquist (J-N) noise (see, for example, Ref. [27]). Indeed, the J-N noise is $i_{i,J-N}^2 = (4T_0/\rho)\delta f$, while the dark current noise is $i_{n,dark}^2 = 4eJ^{dark}\delta f = (eV_G/\rho)\delta f$, for the ratio of the pertinent detectivity values we obtain $D^*/D_{J-N}^* \simeq \sqrt{T_0/eV_G}$. However, the optimum value of

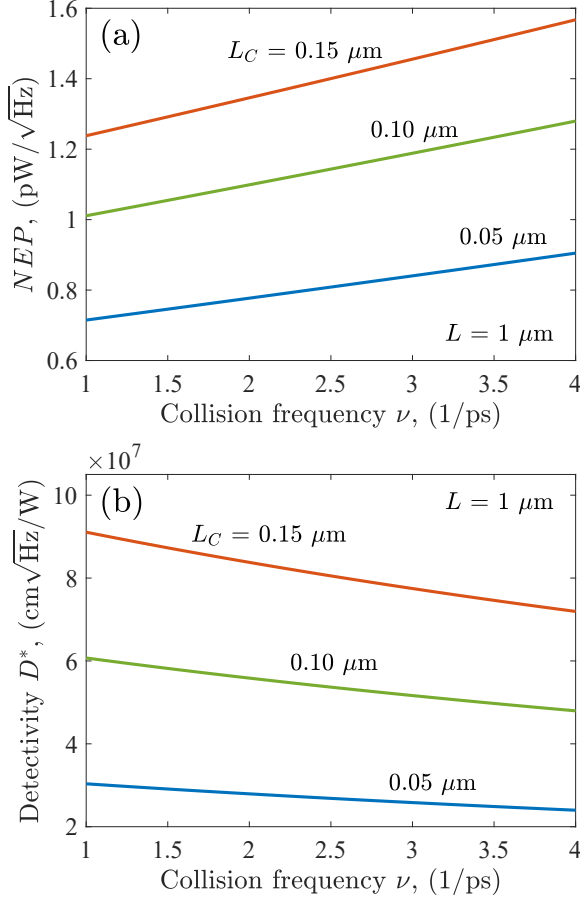


FIG. 7. Dependencies of (a) noise equivalent power (NEP) and (b) dark current limited detectivity D^* on the collision frequency ν calculated for the GC-FETs with different lengths L_C of the b-P collector window BL at the resonant frequency ($\omega = \Omega_P$).

the gate bias would also depend on the exposure level and the readout circuitry (see Ref. [28] for more details).

The present study does not include the consideration of high bias voltages since, in this case, the "thermionic model" becomes invalid and the electron tunneling from the GC through the b-P BL must be accounted for.

The parameters assumed above correspond to the electron mobility in the GC in the range of $\mathcal{M} \simeq (1.78 - 7.14) \times 10^4 \text{ cm}^2/\text{V}\cdot\text{s}$. For the chosen electron density, these values for the room temperature mobility in the GCs, a substantial part of which is encapsulated by b-BN, are fairly realistic (see, for example, Refs. [11–13]). The elevated values of the GC room-temperature mobility and, hence, decreased electron collision frequencies, can be also achieved in the GC-FET structures with the sections of the WSe_2 gate BL [29] replacing the pertinent h-BN sections. Similar GC-FET bolometric detectors can comprise the b-AsP or b-As central BL sections.

Below we compare the voltage responsivities, $R_{\Omega_P}^V$ and $R_{\Omega_P}^{V*}$, of the GC-FET detectors with the composite h-

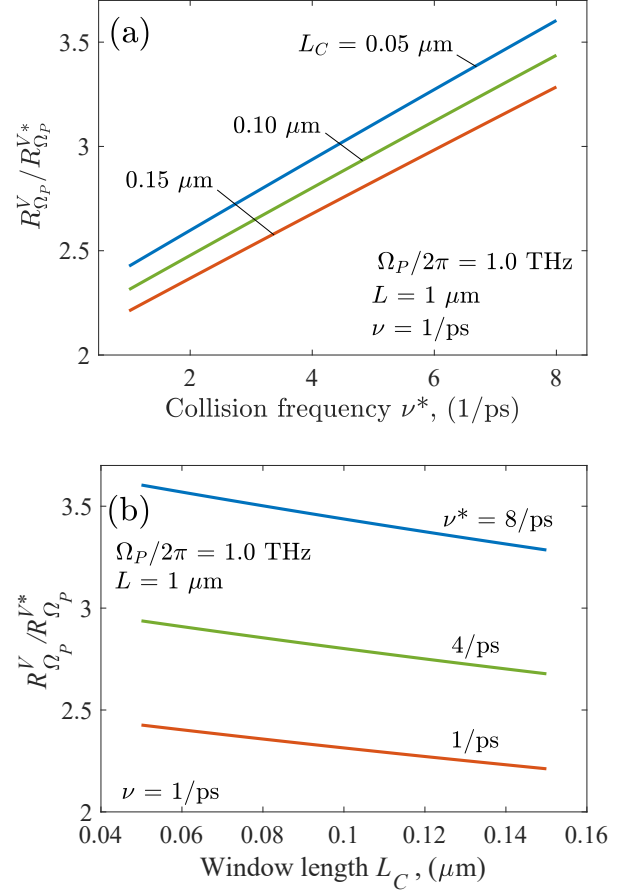


FIG. 8. Ratio of the responsivities, $R_{\Omega_P}^V/R_{\Omega_P}^{V*}$, of GC-FET detectors with the composite h-BN/b-P/h-BN gate BL and with the b-P gate BL (a) as a function of the electron collision frequency ν^* for different L_C and (b) as a function of L_C for different ν^* (at $\nu = 1/\text{ps}$ and $L = 1.0 \mu\text{m}$).

BN/b-P/h-BN gate BL and the uniform b-P gate BL [15] at $\omega = \Omega_P$, assuming that the load resistances are equal to their terminal resistances for both detectors. For their responsivities, we obtain the plots in Fig. 8 (the asterisk marks the responsivity of the GC-FETs with the b-P gate BL). Figure 8(a) shows the ratio of the responsivities $R_{\Omega_P}^V/R_{\Omega_P}^{V*}$, as a function of the collision frequency, ν^* , in the GC-FETs with the b-P gate BL, for the the collision frequency in the FET with the composite BL equal to $\nu = 1/\text{ps}$ and different b-P window BL length values L_C . Figure 8(b) shows the dependence of these responsivities on L_C calculated for different ν^* . As seen in Fig. 8, the incorporation of the composite gate BL might provide a marked enhancement of the GC-FET detector performance. The fact that the ratio $R_{\Omega_P}^V/R_{\Omega_P}^{V*}$ increases with increasing ν^*/ν relatively slowly is attributed to a weakening of the electron cooling at the side contacts when ν^* rises.

When electron collision frequency in the GC central (collector window) section $\nu_C \gg \nu$, the contribution of

this section to the Joule heating can be marked. This might limit the applicability of the model used above to a relatively small L_C/L .

Now we compare the net Joule power produced in the side sections, $2L\langle Q_\omega \rangle$, and in the central section, $2L_C\langle Q_{\omega,C} \rangle$, at the fundamental plasmonic resonance $\omega = \Omega_P$ for the limiting case $\nu \ll \Omega_P \lesssim \nu_C$. Equations (A3) and (A4) (see Appendix A) give rise to the following estimate of the ratio:

$$\frac{L\langle Q_\omega \rangle}{L_C\langle Q_{\omega,C} \rangle} \simeq \frac{\nu^2}{\nu_C^2} \sqrt{\frac{\nu_C^2 + \omega^2}{\nu^2 + \omega^2}} \times \left| \frac{\cos(\gamma_{\omega,C} L_C/L)}{\cos(\gamma_\omega L_C/L)} \right|^2 \frac{\int_{-L}^L dx |\sin(\gamma_\omega x/L)|^2}{\int_{-L_C}^{L_C} dx |\sin(\gamma_{\omega,C} x/L)|^2}. \quad (15)$$

At the fundamental plasmonic resonance ($\omega = \Omega_P$), assuming that $\nu \ll \Omega_P \lesssim \nu_C$, Eq. (15) yields the estimate:

$$\frac{L\langle Q_\omega \rangle}{L_C\langle Q_{\omega,C} \rangle} \simeq \left(\frac{\nu}{\nu_C} \right)^2 \left(\frac{L}{L_C} \right)^3. \quad (16)$$

This implies that the simplification made in Sec. IV is justified when $L_C/L \ll (\nu/\nu_C)^{2/3} \simeq (M_C/M)^{2/3}$. Here M and M_C are the electron mobilities in the pertinent sections of the GC. In the case of the h-BN/b-P/h-BN composite BL at room temperature, one can set $M_C \simeq 8 \times 10^3 \text{ cm}^2/\text{Vs}$ [10], and $M \simeq (3-6) \times 10^4 \text{ cm}^2/\text{Vs}$ [11] (i.e., $\nu \simeq (2-3)/\text{ps}$ as was used for the dependences in Figs. 3-5). The latter values correspond to the condition $L_C/L < 0.26-0.41$, which was satisfied in the above calculations. At a small L_C/L and a large ν_C , the electron heating in the middle section can be not too small. However, this circumstance can be beneficial leading to the enhancement of the GC-FET bolometric detectors under consideration.

Our device model intended for the GC-FET bolometric detectors with the composite BL assumes that the effect of Peltier cooling is weaker than the electron energy relaxation due to the interaction with phonons. The pertinent condition means $(L_C/L)(\tau_\epsilon/\tau_\perp)(\Delta_C\Delta_M/T_0^2)\exp(-\Delta_M/T_0) \ll 1$. Using the parameters listed in Table I, we arrive at the following criterion $L_C/L \ll \tau_\perp/\tau_\epsilon$. If $\tau_\perp \lesssim \tau_\epsilon$, this condition is not burdensome.

The effect of the electron thermal transport along the GC and of the side contacts cooling can be diminished in the GC structures shown in Fig. 1(c). In the structure with a short b-P window BL and a short MG shown in Fig. 1(c), the spacing $2L$ can be relatively large without sacrificing the plasmonic frequency Ω_P . This is because the ungated GCs can exhibit rather large Ω_P even at relatively long $2L$. The device model of this GC-FET bolometric detector is more complex and requires a separate study.

CONCLUSIONS

We predicted that implementation of the GC-FET bolometric detectors with the composite h-BN/b-P/h-BN gate BL having a narrow b-P collector window could substantially enhance the detector performance in comparison with the GC-FETs with the uniform b-P gate BL, especially invoking the plasmonic resonances.

AUTHOR'S CONTRIBUTIONS

All authors contributed equally to this work.

ACKNOWLEDGMENTS

The work at RIEC, UoA, and UB was supported by the Japan Society for Promotion of Science (KAKENHI Nos. 21H04546, 20K20349), Japan and the RIEC Nation-Wide Collaborative research Project No. R04/A10, Japan. The work at RPI was supported by AFOSR (contract number FA9550-19-1-0355).

CONFLICT OF INTEREST

The authors declare no conflict of interest.

DATA AVAILABILITY

All data that support the findings of this study are available within the article.

APPENDIX A.

The signal component of the potential $\delta\varphi_\omega$ in the gated GC is governed by the following equations [6, 15]:

$$\frac{d^2\delta\varphi_\omega}{dx^2} + \gamma_\omega^2\delta\varphi_\omega = 0 \quad (A1)$$

at $L_C < |x| < L$, and

$$\frac{d^2\delta\varphi_\omega}{dx^2} + \gamma_{\omega,C}^2\delta\varphi_\omega = 0 \quad (A2)$$

at $0 \leq |x| < L_C$. Here $\gamma_\omega = \pi\sqrt{\omega(\omega + i\nu)}/2\Omega_P$, $\gamma_{\omega,C} = \pi\sqrt{\omega(\omega + i\nu_C)}/2\Omega_P$, and ν and ν_C are the electron collision frequencies in the pertinent section of the GC. Apart from the boundary conditions (3), these equations are supplemented by the conditions of the potential continuity at $x = \pm L_C$.

In the case $L_C \ll L$, neglecting the contribution of a narrow region $-L_C < x < L_C$, i.e., extending the validity

of Eq. (A1) all over the whole GC, we obtain

$$\delta\varphi_\omega = \delta V_\omega \frac{\cos(\gamma_\omega x/L)}{\cos \gamma_\omega}. \quad (\text{A3})$$

This equation leads to Eq. (4) in the main text.

The electron collision frequency in the b-P collector window region ν_C differs from that, ν , in the main part of the GC-FET structure, where it is determined by the GC-n-BN interfaces. In the devices under consideration, the ratio ν_C/ν can be rather large. Solving Eqs. (A1)

and (A2), we obtain the spatial potential distribution in the region $L_C < |x| < L$ coinciding with that given by Eq. (A3), while the distribution in the region $-L_C < x < L_C$ is given by

$$\delta\varphi_\omega = \delta V_\omega \frac{\cos(\gamma_{\omega,C} x/L)}{\cos \gamma_{\omega,C}} \frac{\cos(\gamma_\omega L_C/L)}{\cos(\gamma_{\omega,C} L_C/L)}. \quad (\text{A4})$$

If $\nu_C = \nu$, Eqs. (A3) and (A4) coincide, and Eqs. (4)-(12) are valid for a wide range of ratio L_C/L .

-
- [1] Xi Ling, H. Wang, S. Huang, F. Xia, and M. S. Dresselhaus, "The renaissance of black phosphorus," *PNAS* **122**, 4523 (2015).
 - [2] F. Xia, H. Wang, and Y. Jia, "Rediscovering black phosphorus as an anisotropic layered material for optoelectronics and electronics," *Nat. Commun.* **5**, 4458 (2014).
 - [3] Y. Cai, G. Zhang, and Y.-W. Zhang, "Layer-dependent band alignment and work function of few-layer phosphorene," *Sci. Rep.* **4**, 6677 (2015).
 - [4] F. Liu, X. Zhang, P. Gong, T. Wang, K. Yao, S. Zhu, and Y. Lu, "Potential outstanding physical properties of novel black arsenic phosphorus $\text{As}_{0.25}\text{P}_{0.75}/\text{As}_{0.75}\text{P}_{0.25}$ phases: a first-principles investigation," *RSC Adv.* **12**, 3745 (2022).
 - [5] V. Ryzhii, C. Tang, T. Otsuji, M. Ryzhii, V. Mitin, and M. S. Shur, "Hot-electron resonant terahertz bolometric detection in the graphene/black-AsP field-effect transistors with a floating gate," *J. Appl. Phys.* **133**, 174501 (2023).
 - [6] V. Ryzhii, C. Tang, T. Otsuji, M. Ryzhii, V. Mitin, and M. S. Shur, "Effect of electron thermal conductivity on resonant plasmonic detection in the metal/black-AsP/graphene FET terahertz hot-electron bolometers," *Phys. Rev. Appl.* ..., (2023)- in press [arXiv:2303.08492 (2023)].
 - [7] V. Ryzhii, A. Satou, and T. Otsuji, "Plasma waves in two-dimensional electron-hole system in gated graphene heterostructures," *J. Appl. Phys.* **101**, 024509 (2007).
 - [8] A. V. Muraviev, S. L. Rumyantsev, G. Liu, A. A. Balandin, W. Knap, and M. S. Shur, "Plasmonic and bolometric terahertz detection by graphene field-effect transistor," *Appl. Phys. Lett.* **103**, 181114 (2013).
 - [9] V. Ryzhii, T. Otsuji, and M. S. Shur, "Graphene based plasma-wave devices for terahertz applications," *Appl. Phys. Lett.* **116**, 140501 (2020).
 - [10] Y. Liu, *et al.* "Mediated colossal magnetoresistance in graphene/black phosphorus heterostructures," *Nano Lett.* **18**, 3377 (2018).
 - [11] A. S. Mayorov, R. V. Gorbachev, S. V. Morozov, L. Britnell, R. Jalil, L. A. Ponomarenko, P. Blake, K. S. Novoselov, K. Watanabe, T. Taniguchi, and A. K. Geim, "Micrometer-scale ballistic transport in encapsulated graphene at room temperature," *Nano Lett.* **11**, 2396 (2011).
 - [12] H. Hirai, H. Tsuchia, Y. Kamakura, N. Mori, and M. Ogawa, "Electron mobility calculation for graphene on substrates," *J. Appl. Phys.* **116**, 083703 (2014).
 - [13] M. Yankowitz, *et al.* "Van der Waals heterostructures combining graphene and hexagonal boron nitride," *Nat. Rev. Phys.* **1**, 112 (2019).
 - [14] Y. Zhang and M. S. Shur, "Collision dominated, ballistic, and viscous regimes of terahertz plasmonic detection by graphene," *J. Appl. Phys.* **129**, 053102 (2021).
 - [15] V. Ryzhii, C. Tang, T. Otsuji, M. Ryzhii, V. Mitin, and M. S. Shur, "Resonant plasmonic detection of terahertz radiation in field-effect transistors with the graphene channel and the black- $\text{As}_x\text{P}_{1-x}$ gate layers," *Sci. Rep.* (2023), submitted.[arXiv:2304.11635 (2023)]
 - [16] J. F. Rodriguez-Nieva, M. S. Dresselhaus, L. S. Levitov, "Thermionic emission and negative dI/dV in photoactive graphene heterostructures," *Nano Lett.* **15**, 145 (2015).
 - [17] J. H. Strait, H. Wang, S. Shivaraman, V. Shields, M. Spencer, and F. Rana, "Very slow cooling dynamics of photoexcited carriers in graphene observed by optical-pump terahertz-probe spectroscopy," *Nano Lett.* **11**, 4902 (2011).
 - [18] V. Ryzhii, M. Ryzhii, V. Mitin, A. Satou, and T. Otsuji, "Effect of heating and cooling of photogenerated electron-hole plasma in optically pumped graphene on population inversion," *Jpn. J. Appl. Phys.* **50**, 094001 (2011).
 - [19] V. Ryzhii, T. Otsuji, M. Ryzhii, M. Ryzhii, N. Ryabova, S. O. Yurchenko, V. Mitin, and M. S. Shur, "Graphene terahertz uncooled bolometers," *J. Phys. D: Appl. Phys.* **46**, 065102 (2013).
 - [20] D. Golla, A. Brasington, B. J. LeRoy, and A. Sandhu, "Ultrafast relaxation of hot phonons in graphene-hBN heterostructures," *APL Mater.* **5**, 056101 (2017).
 - [21] K. Tamura, C. Tang, D. Ogiura, K. Suwa, H. Fukidome, Y. Takida, H. Minamide, T. Suemitsu, T. Otsuji, and A. Satou, "Fast and sensitive terahertz detection in a current-driven epitaxial-graphene asymmetric dual-grating-gate FET structure," *APL Photonics* **7**, 126101 (2022).
 - [22] T. Y. Kim, C.-H. Park, and N. Marzari, "The electronic thermal conductivity of graphene," *Nano Lett.* **16**, 2439 (2016).
 - [23] Z. Tong, A. Pecchia, C. Yam, T. Dumitrică, and T. Frauenheim "Ultrahigh electron thermal conductivity in T-Graphene, Biphenylene, and Net-Graphene," *Adv. Energy Mater.* **12**, 2200657 (2022)
 - [24] R. E. Collin *Antenna and Radiowave Propagation* (New York, McGraw-Hill, 1985).
 - [25] A. Rogalski, "Semiconductor detectors and focal plane arrays for far-infrared imaging," *Opto-Electron. Rev.* vol. 21, 406 (2013).

- [26] A. Rogalski, M. Kopytko, and P. Martyniuk, “Two-dimensional infrared and terahertz detectors: Outlook and status,” *Appl. Phys. Rev.* **6**, 021316 (2019).
- [27] L. P. Pitaevskii and E.M. Lifshitz, *Statistical Physics, Part 2: Theory of the Condensed State Vol. 9, Chapter VIII* (Butterworth-Heinemann, 1980).
- [28] V. Mackowiak, J. Peupelmann, Yi Ma, and A. Gorges, “NEP – noise equivalent power [White paper],” https://www.thorlabs.com/images/TabImages/Noise_Equivalent_ accessed 1 June 2023.
- [29] L. Banszerus, T. Sohler, A. Epping, F. Winkler, F. Libisch, F. Haupt, K. Watanabe, T. Taniguchi, K. Müller-Caspary, N. Marzari, F. Mauri, B. Beschoten, and C. Stampfer, “Extraordinary high room-temperature carrier mobility in graphene-WSe₂ heterostructures,” arXiv:1909.09523v1.